

magnitude of the depression in the luminescence yield by the addition of B is reduced.

The second concept that we invoke is required in order to explain the origin of very peculiar effects on the luminescence behavior of these systems caused by lowering the concentration of T from 10^{-2} to 10^{-3} M. It is suggested that there exists two states of C that can transfer electronic energy to B and/or T. One of these is the emitting state of C (i.e., C^*), and the other is a much longer lived state of C (i.e., C^\dagger) that is generated from C^* and is tentatively identified as the lowest triplet state of C.³⁸ Since C^\dagger derives from C^* , the sensitization of B and T by C^\dagger will become increasingly important as the B and T concentrations are reduced. Because C^\dagger is so long-lived, the luminescence intensity of T becomes very sensitive to the presence of O_2 at low concentrations of T.

The luminescence behavior of the three-component system excited with β^- particles is found to be very similar to the behavior observed with optical excitation, at least for B concentrations less than ≈ 0.01 M. From this it is concluded that with ionizing radiation a substantial fraction of the yield of T^* derives from

(38) The identification of C^\dagger with the lowest triplet state of C remains uncertain. Certainly its longer lifetime than C^* cannot be attributed to differences in radiative rate constants since both the singlet and triplet decay channels of saturated hydrocarbons are most plausibly dominated by dissociation to H_2 and/or H atom. On the other hand, we require C^\dagger to be a state to which C^* can decay (i.e., it should lie lower than C^*) and both theoretical and spectroscopic investigations show the triplet state of saturated hydrocarbons to be within a few tenths of an electronvolt of the C^* state and provide no evidence for any other lower lying transitions (see ref 33).

geminate recombinations of $C^+ + e^-$ to give C^* , which then behave precisely as they do under optical excitation conditions (i.e., to transfer energy to B and/or T). However, deviations from optical behavior begin to develop at higher concentrations of B. In the case of B = benzene, the β^- -particle-irradiated solutions, when studied as a function of B concentration, recover their initial loss in χ at lower concentrations of B than is observed under optical-excitation conditions. This "upswing" in χ , which ultimately gives rise to what has usually been called the "luminescence minimum", derives not from the concentration dependence of the B internal-conversion efficiency nor from direct excitation of B (both of which cause "upswing" at much larger concentrations of B) but rather is caused by specific ionic channels involving the geminate recombinations $C^+ + B + e^- \rightarrow C + B^+ + e^- \rightarrow C + B^*$ and $C^+ + B + T + e^- \rightarrow C + B^+ + T^- \rightarrow C + B + T^*$. Analysis of the data indicates that $B^+ + e^- \rightarrow B^*$ is inefficient when B = toluene and that inefficiencies may also exist in the $B^+ + T^- \rightarrow B + T^*$ process for B = both benzene and toluene.

Acknowledgment. This research was supported in part by the U.S. Department of Energy, Division of Chemical Science, Office of Basic Energy Sciences. We are also grateful to David Tweeten for useful discussions and to both him and David B. Johnston for their technical assistance.

Registry No. TMPD, 100-22-1; PPO, 92-71-7; O_2 , 7782-44-7; N_2 , 7727-37-9; β^- , 12587-47-2; cyclohexane, 110-82-7; *trans*-decalin, 493-02-7; methylcyclohexane, 108-87-2; bicyclohexyl, 92-51-3; *n*-heptane, 142-82-5; 2,3-dimethylbutane, 79-29-8; benzene, 71-43-2; toluene, 108-88-3; *p*-terphenyl, 92-94-4.

Picosecond Resonant Energy Transfer Studies of Aqueous Anionic Micellar Solutions

Kee-Ju Choi,* Leonid A. Turkevich,*[†] and Roman Loza

BP America,[‡] Corporate Research Center, 4440 Warrensville Center Road, Cleveland, Ohio 44128
(Received: October 8, 1987)

Time-resolved resonant energy transfer between donor (rhodamine 6G) and acceptor (malachite green) dye molecules solubilized in micelles is used to study micellar size and shape. Single-photon counting or frequency-conversion optical gating provides our picosecond time profile. The dyes are solubilized at the spherical surface of sodium dodecyl sulfate micelles. At 0.3 M NaCl, the aggregation number $N = 118$, with the fits being extremely sensitive to micelle size, shape, and solubilization location of the dyes. Resonant energy transfer is also applied to aqueous solutions of ethoxylated sulfonates. The aggregation number grows (from $N \sim 40$) with salt: the spherical micelles distort to flexible, polymeric micelles. The picosecond energy transfer provides direct evidence for this shape change.

1. Introduction

Self-association into organized structures is an integral property of surfactants in solution.¹ In aqueous solution, the micellar aggregates exhibit a variety of shapes depending on surfactant concentration, salinity, and temperature. The microscopic studies of these aggregates influences many of their macroscopic solution properties. A detailed microscopic study of the structure of these surfactant aggregates is essential for any theoretical understanding of these self-associating solutions. This paper describes our application of (singlet) fluorescence probe methods (with radiative lifetimes $\tau_R < 500$ ns) in the study of surfactant aggregation behavior in aqueous solution.²

The photophysical properties of many organic dyes are sensitive to changes in their microenvironments. The chemistry of the probe determines its microscopic solubilization site. Rhodamine 6G and malachite green exemplify cationic probes that solubilize at the

surface of anionic micelles.^{4,5} However, cationic dyes can form insoluble complexes with the anionic surfactants at surfactant concentrations close to the critical micelle concentration (cmc). This complicates the analysis of fluorescence probe measurements in the sub- and near-cmc regimes. Fortunately, however, these dyes redissolve at higher surfactant concentrations, which enables their use in the study of micellar structure well above the cmc. The probe dyes themselves also mutually aggregate: large organic dyes are known^{6a} to form dimers and larger aggregates at high

(1) *Micellization, Solubilization and Microemulsions*; Mittal, K. L., Ed.; Plenum: New York, 1977.

(2) Turro, N. J.; Gratzel, M.; Brown, A. M. *Angew. Chem., Int. Ed. Engl.* **1980**, *19*, 675. Singer, L. A. In *Solution Behavior of Surfactants*; Mittal, K. L., Fendler, E. J., Ed.; Plenum: New York, 1982; Vol. 1, p 73.

(3) Forster, Th. *Z. Naturforsch., A: Astrophys., Phys., Phys. Chem.* **1949**, *4A*, 321. *Ann. Phys. (Leipzig)* **1948**, *2*, 55. *Discuss. Faraday Soc.* **1959**, *27*, 7.

(4) Kasatani, K.; Kawasaki, M.; Sato, H.; Nakashima, N. *J. Phys. Chem.* **1985**, *89*, 545.

(5) Klein, U. K. A.; Haar, H. P. *Chem. Phys. Lett.* **1978**, *58*, 531.

* Also at Department of Physics, Case Western Reserve University, Cleveland, OH 44106.

[‡] Formerly The Standard Oil Company.

local concentrations. In our measurements, dimer formation is not a problem as we have been careful always to maintain low local dye concentrations.

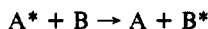
In section 2, we review the Förster theory³ of resonance energy transfer and its application to micellar systems. In section 3, we outline the experimental technique involved in measuring picosecond fluorescence decay dynamics. In section 4, we test the technique with results on a well-known model surfactant system, sodium dodecyl sulfate (SDS), and compare these with results in the literature. In section 5, we present our results on a branched-tail ethoxylated sulfonate, sodium 2-[2-(2-hexyldecyl-oxy)ethoxy]ethanesulfonate (C₁₆EO₂), and discuss evidence for a transition from small spherical to large flexible, polymeric-like micelles.

2. Resonance Energy Transfer

For two different species (A, B) of dye molecules coexisting in solution, the fluorescence intensity from the molecule (A) with the higher excitation energy



decreases in time due to the transfer of excitation energy to the other molecule (B) with the lower excitation energy



The Förster rate k of dipole-dipole resonance energy transfer is given by³

$$k = (1/t_0)(R_0/R_{AB})^6$$

where t_0 is the fluorescence decay time of A alone in solution (actually the sum of the rates of all non-energy-transfer deactivation processes, including, of course, the spontaneous emission) and R_{AB} is the distance between the two molecules A and B; clearly $k(R_0) = 1/t_0$. The characteristic distance R_0 can be expressed⁵ in terms of experimental quantities

$$R_0^6 = \frac{9000 \ln 10}{128\pi^2 n^4 N} k_p^2 \int_0^\infty F(\nu)A(\nu) \frac{d\nu}{\nu^4} \quad (1)$$

$F(\nu)$ is the fluorescence intensity, $A(\nu)$ is the absorption intensity, N is Avogadro's number, and n is the refractive index of the solution. k_p is the orientation factor

$$k_p = \cos \phi_{AB} - 3 \cos \phi_A \cos \phi_B$$

where ϕ_{AB} is the angle between the transition moment vectors of A and B, and ϕ_A and ϕ_B are the angles between these vectors and the direction $\vec{r}_A - \vec{r}_B$. For a random directional distribution, $\langle k_p^2 \rangle = 2/3$.

The probability p_A that the excitation remains on the molecule A is given by

$$-dp_A/dt = 1/t_0 + (1/t_0)(R_0/R)^6 \quad (2)$$

Integrating (2), with initial condition $p_A(0) = 1$, yields

$$p_A(t) = \exp\{-[t/t_0 + (t/t_0)(R_0/R)^6]\} \quad (3)$$

i.e., the population of excited A molecules decays with single-exponential kinetics.

We now consider the statistical distribution of distances R . Let $r(R)$ be the probability that a B molecule is found at the distance R from the excited A molecule; then the average excitation probability $\langle p_A \rangle$ becomes

$$\langle p_A(t) \rangle = \exp(-t/t_0) \int \exp[-(t/t_0)(R_0/R)^6] r(R) dR \quad (4)$$

Therefore, the observed decay kinetics gives information as to the distribution of the quencher molecule B. By assuming various models for the quencher distribution, it is possible to investigate the structure of the system of interest. We summarize below the

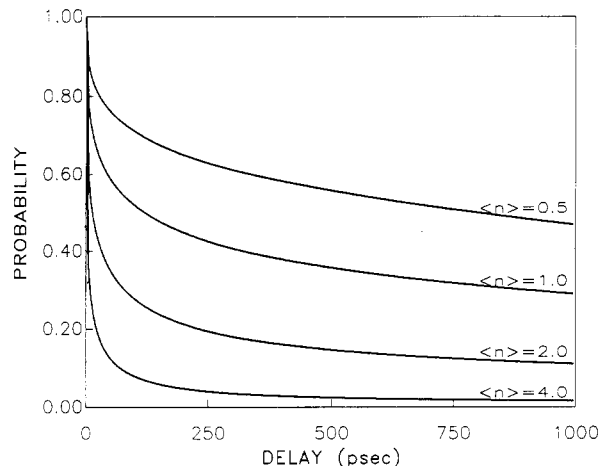


Figure 1. Simulated fluorescence time profiles for the rhodamine 6G/malachite green pair, at fixed micelle radius $R_m = 20 \text{ \AA}$, for various quencher concentrations $\langle n \rangle$: 0.5, 1.0, 2.0, and 4.0. $\langle n \rangle$ primarily determines the final fluorescence intensity reached after a few hundred picoseconds.

decay kinetics for cationic dyes distributed in spherical anionic micelles.

Rhodamine 6G (with^{6b} radiative lifetime $\tau_R \sim 4 \text{ ns}$) and malachite green form a useful donor-acceptor pair for the resonance energy transfer measurements, because this pair has a critical transfer distance $R_0 \sim 52 \text{ \AA}$, comparable to the micellar sizes under investigation (N.B. this R_0 is large compared to other possible probe dye combinations, which are thus less sensitive in the 50- \AA range). A large critical transfer distance allows one to measure a large aggregate size.

When cationic dyes, such as rhodamine 6G and malachite green, are used as donor and acceptor in an anionic micellar solution, both dyes are likely to adsorb at the micellar surface. The probability, $r(R) dR$, of finding an acceptor at distance R from a donor is proportional⁴ to R . Using this probe distribution, expression 4 for the time profile for a micelle, which contains one donor and one acceptor, becomes

$$\langle p_A(t) \rangle = \exp(-t/t_0) \int_0^{2R_m} \exp[-(t/t_0)(R_0/R)^6] R dR \quad (5)$$

In (5), R_m is the radius of the micelle.

Since we only measure an average value of fluorescence decay time profiles, we must consider the distribution of probe dye molecules over many micelles. The probability of finding a micelle with n probe dye molecules is given⁷ by the Poisson distribution

$$p(n) = \langle n \rangle^n e^{-\langle n \rangle} / n! \quad (6)$$

where $\langle n \rangle = [\text{acceptor dye}]/[\text{micelle}]$. Combining (5) and (6), we obtain

$$P_A(t) = \exp(-t/t_0) \sum_n \frac{\langle n \rangle^n e^{-\langle n \rangle}}{n!} \left\{ \int_0^{2R_m} \exp[-(t/t_0)(R_0/R)^6] R dR \right\}^n \quad (7)$$

The above derivation neglects the donor-donor energy-transfer rate; the donor concentration does not appear in this calculation. This approximation should be valid in the regime where no micelles contain more than one donor. In our experiments, we have limited the donor concentration so that $[\text{donor}]/[\text{micelle}] < 0.1$. Figure 1 shows a series of time profiles, calculated with (7), as a function of $\langle n \rangle$ at fixed micelle radius $R_m = 20 \text{ \AA}$. In Figure 1, we have used the photophysical constants for the rhodamine 6G/malachite green pair. The varying acceptor dye concentration $\langle n \rangle$ determines the final fluorescence intensity reached after a few hundred picoseconds. This happens because all the excited donors in those micelles with at least one acceptor are quenched by the resonance

(6) (a) Selwyn, J. E.; Steinfeld, J. I. *J. Phys. Chem.* **1972**, *76*, 762. (b) Berlman, I. B. *Handbook of Fluorescence Spectra of Aromatic Molecules*; Academic: New York, 1971; p 412.

(7) Atik, S. S.; Thomas, J. K. *J. Am. Chem. Soc.* **1981**, *103*, 3543. Yekta, A.; Aikawa, M.; Turro, N. J. *Chem. Phys. Lett.* **1979**, *63*, 543.

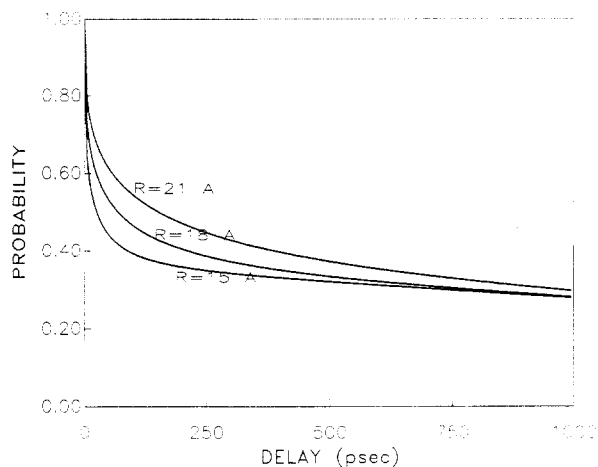


Figure 2. Simulated fluorescence time profiles for the rhodamine 6G/malachite green pair, at fixed quencher concentration $\langle n \rangle = 2.0$, for various micelle radii R_m : 15, 18, and 21 Å. R_m primarily determines the initial decay rate of the fluorescence intensity.

energy transfer within this time scale. Figure 2 shows another series of time profiles, calculated with (7), as a function of R_m at fixed dye concentration $\langle n \rangle = 2.0$, again with the photophysical constants for the rhodamine 6G/malachite green pair. The micelle radius mainly affects the initial decay rate, and the slower decay component remains unchanged. It is evident from Figures 1 and 2 that picosecond measurements can precisely determine both parameters $\langle n \rangle$ and R_m , so long as R_m is not significantly larger than the critical transfer distance R_0 . In the case $R_m \gg R_0$, it is not possible to separate the independent effects of $\langle n \rangle$ and R_m (see below, section 5b).

It should be noted that, for the parameters of the rhodamine 6G/malachite green pair, the resonance energy transfer process is almost completed within the first few hundred picoseconds, and the excited-state population decreases substantially within 50 ps in a typical micellar environment. Due to the fast dipole-dipole interaction rate, diffusion of the probe dye molecules can be neglected. This eliminates the additional collisional quenching mechanism, whose rate is given by the time for dyes to diffuse over micellar distances, which is long on our measurement time scale. In addition, while the structure of surfactant aggregates is dynamic, with surfactant molecules in the aggregate being in dynamic equilibrium with those of other aggregates and with monomers in the bulk solution, with a typical micellar lifetime on the order of milliseconds, these dynamics can again be neglected because resonance energy transfer occurs on such a rapid time scale. Similarly, while the probe dye molecules can also dissociate from the micellar structure and migrate, these dynamics can also be neglected, again because resonance energy transfer is such a rapid process.

Resonance energy transfer permits measurement of both size and concentration of spherical micelles. Since the transfer rate depends on the sixth power of the distance, the time profile is very sensitive to the micellar size. The model described in this section works well when the micellar size is smaller than the critical transfer distance of the donor-acceptor pair used. It should be noted that the radius obtained from this measurement is the radius of the probe dye solubilization site; this must be augmented by the distance of the chromophore from the head group to determine the actual micelle radius. It is possible to control the solubilization site by changing the chemical properties of the probe dyes (e.g., polar vs nonpolar dyes); recognition of the relevant solubilization site is necessary for an intelligent interpretation of micelle radius obtained from a resonance energy transfer measurement.

3. Experimental Section

(a) *Experimental Apparatus.* We have used either time-correlated single-photon counting or frequency-conversion optical gating to obtain our picosecond fluorescence time profiles. The principles and many applications of both methods have been

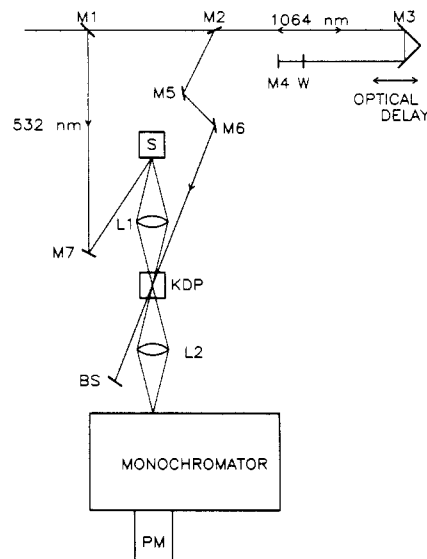


Figure 3. Schematic of the frequency-conversion optical-gating apparatus described in text.

reported in the literature.^{8,9} Optical gating provides the better time resolution, but we have achieved better signal/noise with the single-photon counting. With the former, we are sensitive to fluorescence from dye concentrations as low as 5×10^{-7} M, while with the latter, we are sensitive to even lower dye concentrations. We briefly describe these two experimental setups in this section.

(i) *Time-Correlated Single-Photon Counting.* For the time-correlated single-photon counting experiment,⁸ we use a commercial cavity-dumped synchronously pumped dye laser as a light source. With a rhodamine 110 dye laser, at 540 nm, we have 60-mW average power at 4-MHz repetition rate, with pulse duration typically of 20 ps. We use only $\sim 1\%$ of the available power to excite our samples. A thin film polarizer is mounted on a rotating stage and set at 54.7° to eliminate the effect of rotational diffusion. A polarization scrambler is used in front of a HR-320 monochromator to compensate for the polarization-dependent efficiency of the gratings. We use a 600 g/mm grating to reduce time dispersion in the monochromator. The signal from a 6- μm microchannel plate photomultiplier is amplified with a broadband amplifier (28-dB gain and 4.2-GHz bandwidth). A constant-fraction discriminator (CFD) detects the leading edge and starts a time-to-pulse-height converter (TPHC). Trigger pulses from a fast pin photodiode and another CFD are fed to the stop channel of the TPHC. The counting rate of a single channel is limited to less than 1% of the laser repetition rate to prevent pulse pile-up error. Overall time resolution of this device is 60 ps. The major limiting factor is the dispersion in the monochromator; we have not tried to eliminate the time dispersion any further.

(ii) *Optical Gating.* We have also used frequency-conversion optical gating⁹ to obtain our picosecond fluorescence time profile. The experimental apparatus for these time-resolved fluorescence measurements is shown in Figure 3. An active-passive mode-locked Nd:YAG laser generates 30-ps light pulses at the rate of 10 pulses/s. The wavelength of the laser of 1064 nm. Second (532 nm), third (354.7 nm), and fourth (266 nm) harmonic frequencies are generated with combinations of three nonlinear crystals. With the extremely high peak power of the laser beam (1×10^9 W), the conversion efficiency for harmonic generation is very high ($\sim 60\%$ for 532 nm, 30% for 354.7 nm, and 10% for 266 nm). The sample (S) is excited with a green (532-nm) laser pulse of ~ 30 -ps duration. The resulting fluorescent light is combined with a near-infrared (1064-nm) laser pulse in a nonlinear optical crystal (type II potassium dihydrogen phosphate). The time scanning is provided by passing the probe beam through an

(8) O'Connor, D. V.; Phillips, D. *Time-Correlated Single Photon Counting*; Academic: London, 1984.

(9) (a) Halliday, L. A.; Topp, M. R. *Chem. Phys. Lett.* **1979**, *46*, 8. (b) Choi, K.-J.; Boczar, B. P.; Topp, M. R. *Chem. Phys.* **1981**, *57*, 415.

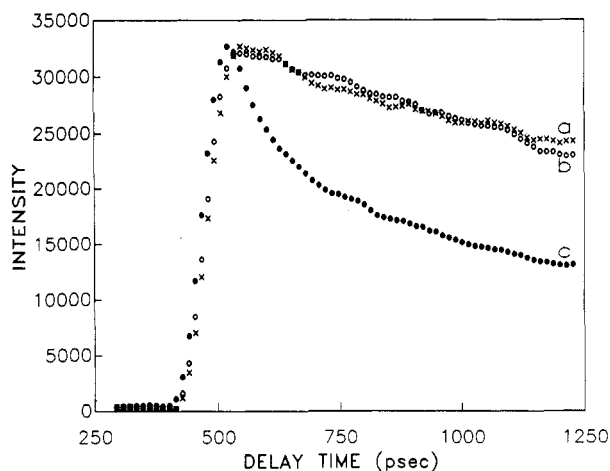


Figure 4. Fluorescence time profiles of rhodamine 6G in (a) water, $\tau = 3300$ ps, (b) water with $[MG] = 0.1$ mM, and (c) water with SDS micelles and MG.

optical delay line, which consists of a moving retroreflector (M3), a thin-film polarizing beam splitter (PL), dielectric mirrors (M5, M6), and a quarter-wave plate (W). Since the double path through the retroreflector compensates small changes in the beam direction, this arrangement provides a very stable optical delay, and the optical alignment is greatly simplified. The generated sum frequency is detected by a monochromator and high-gain photomultiplier. A PDP 11/73 computer with a CAMAC interface performs all the data acquisition and the delay line control.

(b) *Sample Specifications.* We use laser-grade rhodamine 6G and malachite green as the donor and acceptor dyes, respectively, for the resonance energy transfer measurements. The sodium dodecyl sulfate is Fluka puriss grade and is used as received. The ethoxylated sulfonate ($C_{16}EO_2$) is synthesized as described in section 5a. The water used is double-distilled; the sodium chloride is analytical grade.

4. Results for Sodium Dodecyl Sulfate

We have tested our resonance energy transfer method with the model surfactant sodium dodecyl sulfate (SDS). As literature results from almost all known surfactant characterization methods are readily available for SDS micelles in brine solution, it is possible to compare our resonance energy transfer results with those reported by other methods. Without added salt, the cmc for SDS is 8.3 mM; at $[NaCl] = 0.1$ M, the cmc is reduced to 1.5 mM; our measurements are taken at $[NaCl] = 0.3$ M, where the cmc is further reduced to 0.3 mM. Our measurements are for $2 \text{ mM} < [SDS] < 17 \text{ mM}$, all of which are well above the cmc.

Figure 4 shows typical fluorescence time profiles of rhodamine 6G under three different conditions. Rhodamine 6G alone in water (curve a) shows a single-exponential decay with 3300-ps decay time. When 0.1 mM malachite green is added to the solution (curve b), the time profile of the rhodamine 6G changes only slightly, since the overall quencher concentration remains small. However, when SDS is added to the combined solution (curve c), the time profile changes drastically, due to the complete solubilization of the probe dye molecules at the surface of the SDS micelles. Since the volume fraction of micelles in the solution is small, the probe dye is effectively concentrated by its being solubilized in a small portion of the solution. Therefore the quenching rate increases dramatically in a micellar solution. Additional evidence of micellar dye solubilization is indicated by the change in the rhodamine 6G absorption spectrum (Figure 5), where the absorption peak shifts toward the red in a micellar solution. This spectral change has been known¹⁰ as an indication

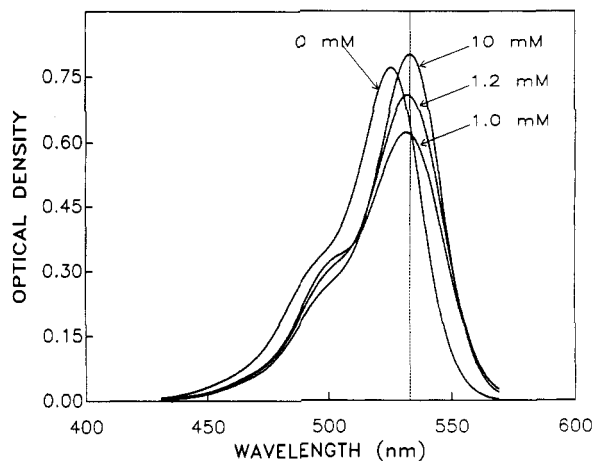


Figure 5. Absorption spectrum of 5×10^{-5} M rhodamine 6G as a function of sodium dodecyl sulfate concentration at $[NaCl] = 0.1$ M. The spectral red shift indicates a strong binding to the micelle.

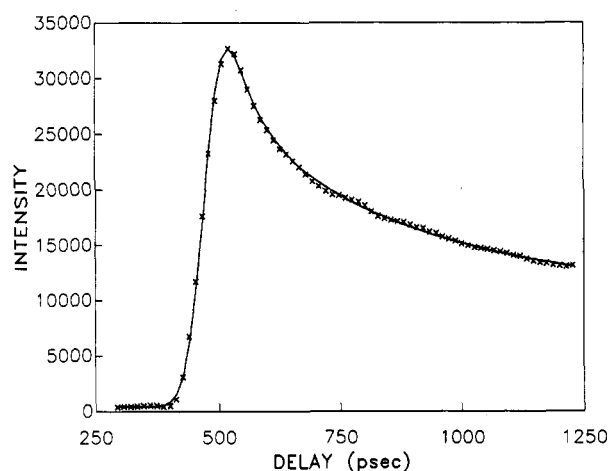


Figure 6. Fluorescence time profile of rhodamine 6G (with malachite green quenchers) in SDS micelles at 0.3 M NaCl, fit with the spherical micelle model; we obtain $\rho = 18$ Å.

of micellization and can be used to measure the critical micelle concentrations of various anionic surfactants. We remark that the short wavelength shoulder is due to dimer formation at the high local dye concentrations present just below the CMC.

Figure 6 shows fluorescence decay data with a calculated time profile assuming a spherical micelle. There is excellent agreement between the experimental data and the model calculation (where R_m and $\langle n \rangle$ are adjustable parameters), confirming the spherical micellar model with the probe dyes solubilized at the micellar surface. An attempt to fit the same data with a homogeneous distribution (i.e., with the dye solubilized throughout the micellar volume) fails. From the curve-fitting parameters, we obtain the micellar radius, $R_m = 22$ Å, and the average number, $\langle n \rangle = 1.60$, of dye molecules per micelle. Since the quencher concentration, $c_q = 6 \times 10^{-5}$ M, and the surfactant concentration, $c_s = 5$ mM, are known, the aggregation number, N_m , can be calculated, using the known cmc = 0.34 mM:

$$N_m = \langle n \rangle (c_s - \text{cmc}) / c_q = 1.60(5.00 - 0.34) / 0.06 = 124$$

Again, we must caution that the radius measured in this experiment is the radius of the dye chromophore solubilization site, because the resonance energy transfer occurs between chromophores. Assuming the rhodamine 6G chromophore to be situated in the water, oriented with its plane normal to the micellar surface, the distance between the cationic head and the center of the chromophore is ~ 3 Å; hence the actual radius of the surfactant head group is ~ 19 Å in 0.3 M NaCl solution. However, if the chromophore lies flat at the micellar surface, the radius of the surfactant head group is 22 Å.

(10) McBain, J. W.; *Colloid Science*; D.C. Heath: Boston, MA, 1950. Mukerjee, P.; Mysels, K. J. *Critical Micelle Concentrations of Aqueous Surfactant Systems*; NSRD-NBS 36; National Bureau of Standards: Washington, DC, 1971; p 9.

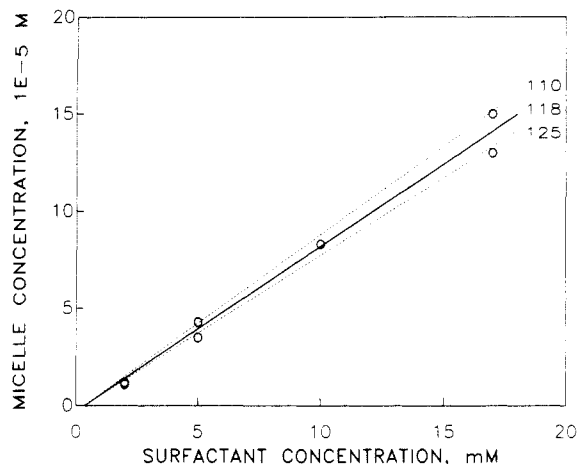


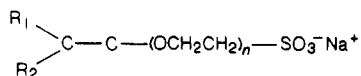
Figure 7. Micelle concentration as a function of SDS concentration; the slope yields the aggregation number $N \sim 118$.

A frequently used method¹¹ to measure micellar aggregation number is based on the fluorescence quenching by either collisional energy transfer or excimer formation. Theoretical treatments and experimental verification of this method have appeared in the literature.^{11–18} This method is capable of measuring the aggregation number and a rate constant which depends on the size and microviscosity of the surfactant core. However, when the aggregate size becomes large ($N > 400$), the measured aggregation number becomes unreliable due to the incomplete fluorescence quenching during the lifetime of the excited probe molecules.

The SDS aggregation number as a function of SDS concentration (at fixed $[\text{NaCl}] = 0.3 \text{ M}$) is shown in Figure 7. The straight line indicates a constant aggregation number of 118, which is the accepted value at this salinity. We have compared our data with N extracted from sedimentation equilibrium combined with isopiestic distillation.^{20,21} We note that this latter method involves an extrapolation to the critical micelle concentration, and it is thus not possible to measure the aggregation number as a function of surfactant concentration. However, when the aggregation number remains constant (as is the case for many ionic surfactants over a wide range of surfactant concentration), these methods may be reliably used. Our resonance energy transfer results directly indicate that the SDS aggregation number does not change in this concentration range.

5. Results for Branched-Tail Ethoxylated Sulfonates

We have also studied the aggregation behavior of branched ethoxylated sulfonates



where R_1 and R_2 represent alkyl tails, with combined carbon number, $m = m_1 + m_2$, in the range $m = 10\text{--}14$, and where $n = 2\text{--}6$ ethoxy units. In this paper, we report our results on the aggregation behavior of $C_{16}EO_2$, i.e., $m_1 = 6$, $m_2 = 8$.

(a) *Preparation.* This surfactant was prepared by using a four-step sequence described below. The reaction of 2-hexyldecyl

methanesulfonate with diethylene glycol is based on a procedure published by Gibson.²²

(i) *Preparation of 2-[2-(2-Hexyldecyloxy)ethoxy]ethanol.* A solution containing 141 g (0.5 mol) of 2-hexyldecanol (Henkel Corp.) in 500 mL of pyridine was cooled to 2 °C in an ice/water bath. To the solution was added dropwise (slowly enough to keep the reaction mixture below 4 °C) 46 mL (68 g, 0.59 mol) of methanesulfonyl chloride. The mixture was allowed to warm to 20 °C for 1 h and then allowed to stand at 10 °C overnight. In the morning the reaction mixture was poured onto 500 mL of concentrated HCl in 600 mL of water. The ice was allowed to melt, and the mixture separated into two layers. The organic layer was removed, and the aqueous layer was washed with 300 mL of petroleum ether. The combined organic layers were washed with 4 M HCl and a saturated salt solution, and dried over anhydrous magnesium sulfate. Removal of the volatiles left behind 144 g (90%) of a yellow oil identified as the 2-hexyldecyl methanesulfonate based on its NMR spectrum.

A 500-mL three-neck round-bottom flask—equipped with a temperature controller, magnetic stirrer, and reflux condenser—was charged with 200 mL of diethylene glycol (170 g, 1.6 mol). To the flask was added 35.2 g (50%, 0.44 mol) of sodium hydroxide solution, and the mixture was heated to 90 °C with stirring for 15 min. To the yellow solution was added dropwise 68.9 g (0.22 mol) of 2-hexyldecyl mesylate. The resultant dark brown solution was stirred for 18 h at 90 °C and then poured into water (1 L), and the organic layer separated. The aqueous layer was extracted with petroleum ether ($2 \times 250 \text{ mL}$), and the combined organic layers were washed with water and a saturated salt solution and then dried over anhydrous sodium sulfate. Removal of the volatiles left behind 65.5 g of a brown oil which was distilled (bp 145–150 °C, 0.15 mmHg) to give 43 g (59%) of a water-white oil identified as 2-[2-(2-hexyldecyloxy)ethoxy]ethanol.

This alcohol was reacted with methanesulfonyl chloride (using the procedure outlined above) to give 53.2 g (100%) of crude 2-[2-(2-hexyldecyloxy)ethoxy]ethyl methanesulfonate. The crude mesylate was taken up in 500 mL of methyl ethyl ketone (MEK) containing 23.4 g (0.16 mol) of sodium iodide. The mixture was heated at reflux for 6 h and then cooled, and the volatiles were removed under reduced pressure. The residue was taken up in 300 mL of petroleum ether and washed with water, a 0.1 M sodium thiosulfate solution, and a saturated salt solution. The volatiles were removed under reduced pressure to give 51.7 g (90%) of an orange oil identified as 1-iodo-2-[2-(2-hexyldecyloxy)ethoxy]ethane on the basis of its NMR spectrum.

(ii) *Preparation of Sodium 2-[2-(2-Hexyldecyloxy)ethoxy]ethanesulfonate.* The crude iodide was added to a solution containing 43.1 g (0.34 mol) sodium sulfite in 340 mL of water and 170 mL of 2-propanol. This two-phase mixture was stirred at reflux for 96 h. The mixture was cooled and extracted with petroleum ether ($2 \times 200 \text{ mL}$). The aqueous (water-2-propanol/surfactant) phase was saturated with sodium chloride. The mixture separated into two layers. The top (2-propanol/surfactant) layer was concentrated (in vacuo) to give a gummy solid. This solid was triturated with acetone, and the acetone was decanted. The residue was taken up in 100 mL of chloroform. The suspension was allowed to settle. The clear chloroform solution was decanted from the precipitated salt. Removal of the chloroform gave a white solid which was dried in vacuo. HPLC (Spectra-Physics Model SP8700, Knauer differential refractometer, Hewlett-Packard Model 3390A recording integrator, and a Waters Associates μ Bondapak C_{18} column using a 10:1 isopropanol-water mixture as the mobile phase at a flow rate of 1.0 mL/min) analysis of this material showed the presence of a single component. Two-phase titration²³ of the product surfactant showed that it contained 98% (of theory) active sulfonate.

(b) *Results.* The aqueous phase diagram is shown in Figure 8. The solubility limits of $\sim 2.5\%$ is essentially unchanged until $[\text{NaCl}] \sim 6 \text{ wt } \%$, whereupon the solubility limit becomes very

- (11) Tachiya, M.; *J. Chem. Phys.* **1982**, *76*, 340.
- (12) Infelta, P. P.; *Chem. Phys. Lett.* **1979**, *61*, 88.
- (13) Gelade, E.; De Schryver, F. C.; *J. Am. Chem. Soc.* **1984**, *106*, 5871.
- (14) Lofroth, J. E.; Almgren, M. In *Solution Behavior of Surfactants*; Mittal, K. L., Fendler, E. J., Eds.; Plenum: New York, 1982; Vol. 1, p 627.
- (15) Lianos, P.; Lang, J.; Straielle, C.; Zana, R.; *J. Phys. Chem.* **1982**, *86*, 1019.
- (16) Lianos, P.; Lang, J.; Strum, J.; Zana, R.; *J. Phys. Chem.* **1984**, *88*, 819.
- (17) Atik, S. S.; Singer, L. A.; *Chem. Phys. Lett.* **1979**, *66*, 234.
- (18) Koglin, P. K. F.; Miller, D. J.; Steinwandel, J.; Hauser, M.; *J. Phys. Chem.* **1981**, *85*, 2363.
- (19) Kusumoto, Y.; Sato, H.; *Chem. Phys. Lett.* **1979**, *68*, 13.
- (20) Kratochvil, J. P.; *J. Colloid Interface Sci.* **1980**, *75*, 271.
- (21) Doughty, D. A.; *J. Phys. Chem.* **1979**, *83*, 2621.

(22) Gibson, T. J.; *Org. Chem.* **1980**, *45*, 1095.

(23) Reid, V. W.; Longman, G. F.; Heinerth, E.; *Tenside* **1967**, *4*, 292–304.

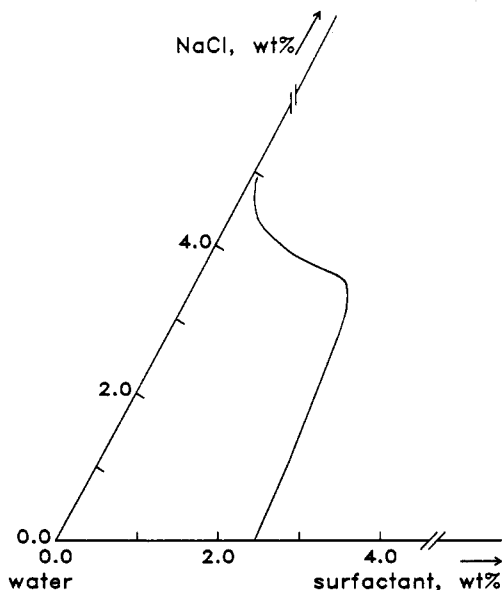


Figure 8. Phase diagram of $C_{16}EO_2$ branched-tail ethoxylated sulfonate with NaCl. The solubility limit is 3% and is unchanged until $[NaCl] = 7\%$, whereupon it becomes very small.

small; concomitantly, at low surfactant concentration, precipitation occurs at $[NaCl] \sim 7$ wt % and is not very sensitive to surfactant concentration. The cmc is also a strong function of salt concentration, dropping precipitously from $\sim 10^{-2}$ without salt to $\sim 10^{-3}$ at $[NaCl] \sim 0.1$ wt %. It is thus expected that salt should affect the aggregation phase behavior of these surfactants. There is no liquid-crystalline phase at the higher surfactant concentrations, the micellar solution remaining isotropic until precipitation. However, the isotropic solution shows a bluish tint at the higher salt concentrations ($[NaCl] > 0.15\%$).

We have studied the aggregation behavior using the picosecond resonant energy transfer techniques described in section 3. We again excite a red-shifted rhodamine 6G and quench with malachite green. Figure 9a shows the time profile we obtain for $[C_{16}EO_2] = 2.5$ mM and $[MG] = 0.05$ mM, along with our two-parameter fit to the data. The fit unambiguously yields a radius of $R_m = 17.5$ Å with an average number of quenchers per micelle $\langle n \rangle = 1.25$. Doubling the quencher concentration to $[MG] = 0.10$ mM (Figure 9b) merely doubles the quencher concentration to $\langle n \rangle = 2.5$ (the solid line is now a prediction from the fit in Figure 9a—i.e., without adjustable parameters), while decreasing the quencher concentration to $[MG] = 0.02$ mM yields (Figure 9c) $\langle n \rangle = 0.5$ (again the solid line is a prediction without adjustable parameters). In summary, without salt, the aggregates of aqueous solution branched-chain ethoxylated sulfonates form spherical micelles, in this case of $R_m = 17.5$ Å.

Figure 10 is a plot of $[micelle]$ vs $[C_{16}EO_2]$ at 0.05 g/dL NaCl concentration. The solid line corresponds to an aggregation number $N = 53$; all the measured points are within experimental error from this line. Thus the aggregate size of $C_{16}EO_2$ does not change as the surfactant concentration increases.

It is instructive to compare the micellar size measured by the resonance energy transfer method with the size of the hydrophobic group estimated from the bond lengths of the hydrocarbon chain. Assuming that the volume of a CH_3 group is 27.4×10^{-24} cm³ and that of a CH_2 group is 26.9×10^{-24} cm³, the radius of a minimum sphere with 53 surfactant molecules is 17.6 Å. This is longer than the maximum length of the hydrocarbon chain (~ 13 Å). The spherical model, however, fits the experimental time profile very well. There are two possible reasons: (i) two ethoxy groups may penetrate the hydrocarbon region and form larger micelles; (ii) the instrumental time resolution is not good enough to measure times shorter than 20 ps, where the energy transfer rate strongly depends on the aggregate size. However, as discussed in section 3, the aggregation number measured by resonance energy transfer should still be accurate, since the micelle size is smaller than the critical Förster transfer distance, R_0 .

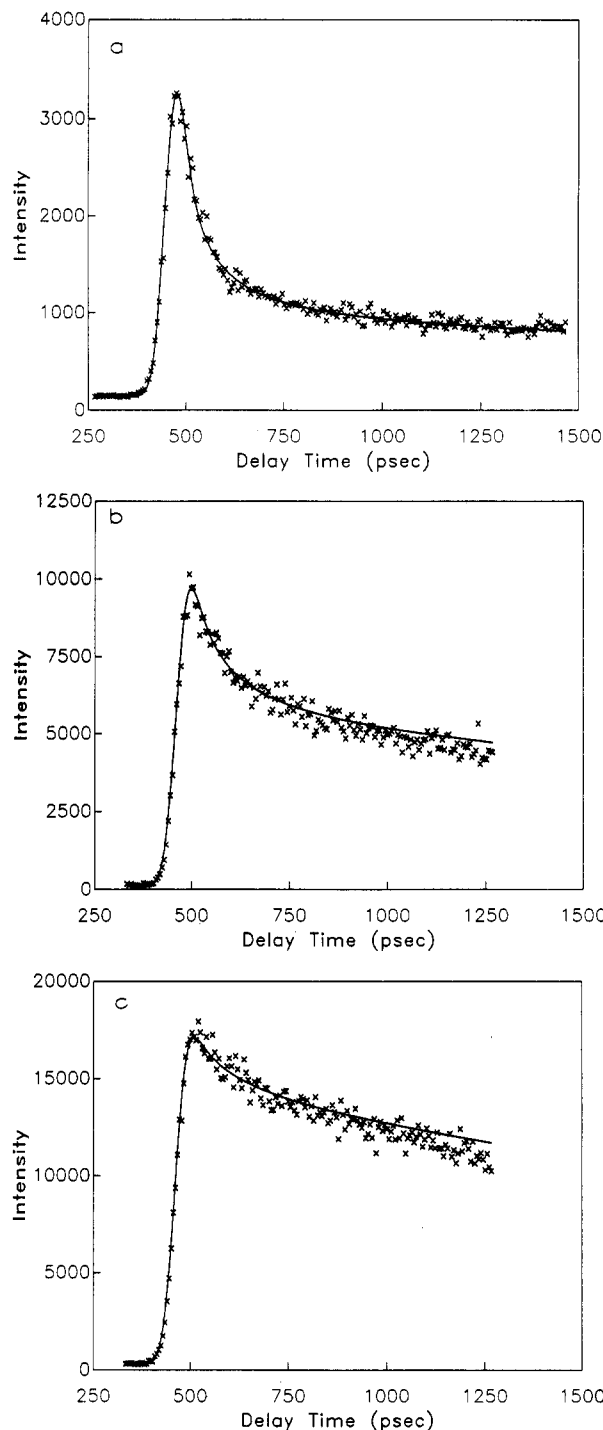


Figure 9. (a) Fluorescence decay profile for rhodamine 6G solubilized in $C_{16}EO_2$ branched-tail ethoxylated sulfonate micelles ($[surfactant] = 2.5$ mM) with $[MG] = 0.05$ mM; $R_m = 17.5$ Å and $\langle n \rangle = 1.25$. (b) The same with $[MG] = 0.1$ mM; $R_m = 17.5$ Å and $\langle n \rangle = 2.5$. (c) The same with $[MG] = 0.02$ mM; $R_m = 17.5$ Å and $\langle n \rangle = 0.5$.

The radius obtained from this experiment is, however, more seriously affected by the model. We obtained a radius of ~ 21 Å for the $C_{16}EO_2$ micelle at $[NaCl] \sim 0.05\%$. Since resonance energy transfer measures the radius of the probe solubilization site, the chemical property of the dye must also be considered. The probes used in this experiment are cationic, but they also contain large hydrophobic groups. The solubilization sites of the probe dyes are believed to be the micellar interfacial region. The 21-Å radius we obtained is too small for a micellar structure where the two ethoxy groups are fully extended toward the solvent phase (i.e., radial ethoxy groups); our results suggest that a large portion of the ethoxy group faces the solvent phase (i.e., tangential ethoxy groups).

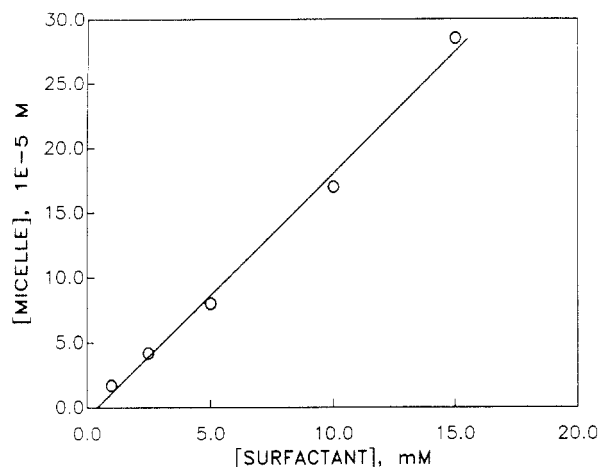


Figure 10. Micelle concentration as a function of $[C_{16}EO_2]$. The solid line corresponds to $N = 53$.

TABLE I: Variation of Hydrodynamic Radius of $C_{16}EO_2$ Micelles with Salt Concentration, As Measured by Bulk Light Scattering

[NaCl], wt %	R_h , Å
0	(18)
0.15	1590 ± 30
1.0	1400 ± 41
2.0	1360 ± 41

We have also studied the effect of salt on the aggregation behavior. The repulsion between the ionic head groups is partially shielded by the counterions, and the head-group area decreases. This change in surfactant-surfactant interaction causes the aggregate size to increase, and the shape of the aggregate is no longer spherical.

With the addition of salt, bulk light scattering indicates a dramatic growth of the aggregates (Table I). For $[NaCl] < 0.15$ wt %, our resonance energy transfer data are consistent with the spherical micellar model with dyes solubilized at the surface. Figure 11 shows the aggregation numbers we have obtained from this study. Consistent with the bulk light scattering, the resonance energy transfer clearly indicates rapid micellar growth in the vicinity of $[NaCl] \sim 0.15$ wt %. The size does not change significantly in the regime 0.03 g/dL $< [NaCl] < 0.10$ g/dL, with a rapid increase at $[NaCl] \sim 0.15$ g/dL. This sharp increase at low salt concentration is somewhat unusual. However, Dahanayake et al.²⁴ have observed anomalous behavior in the single-chain ethoxylated sulfonates and have proposed sodium binding as its origin.

It is impossible to rationalize the large sizes for such giant aggregates (as indicated by the bulk light scattering) without appreciable water penetration into the interior—the model of spherical micelles of a fixed radius ρ with the dye molecules solubilized at the surface is untenable—indeed, we no longer can obtain decent fits with such a model. Instead, we have attempted to fit our fluorescence decay profiles for these giant aggregates to two alternative models. The first is a *vesicle model*, where the micelle is assumed to be a spherical bilayer (of radius R_G) with a water core; the dyes remain solubilized at the surface and thus are confined to a shell, their density scaling as $\rho(R) \sim R$. In this case the time profile is given by

$$F(t) = F_0 \exp[-t/\tau_0 - 1.354n_q(t/\tau_0)^{1/3}(R_0/R_G)^2] \quad (8)$$

The second is a *polymer model*, where the micelle is assumed to be a long cylindrical micelle, so long that it is no longer rigid but undergoes a self-avoiding random walk in order to occupy a sphere (of radius R_G); the dyes again are solubilized at the micellar surface, but as the polymer wanders through the volume R_G^3 , the

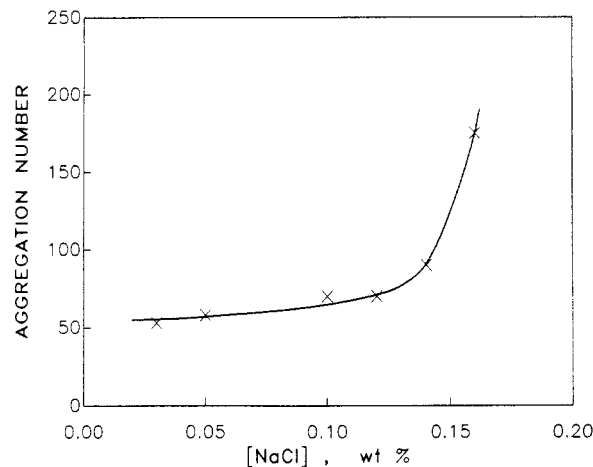


Figure 11. Micelle aggregate size, as measured with resonance energy transfer, as a function of salt at $T = 23$ °C. A rapid increase in micelle radius is observed at $[NaCl] = 0.15$ g/dL. The curve shown is merely a guide through the data points.

TABLE II: Variation of ^{23}Na NMR Line Widths Γ_1 and Γ_2 and Relative Intensity I_1/I_2 with Salt Concentration for $C_{16}EO_2$ Micelles (15 mM)

salt concn, g/dL	Γ_1 , Hz	Γ_2 , Hz	I_1/I_2
[NaCl] = 0.05	15.2 ^a		
[NaCl] = 0.15	31.4	304.2	1.22
[NaCl] = 0.2	24.0	261.5	2.01
[NaCl] = 0.5	26.7	200.8	1.60
[KCl] = 0.2	25.3	265.5	1.23

^a $\Gamma = 7.0$ Hz for ^{23}Na resonance in aqueous solution ($c_s = 0$).

dyes are distributed throughout the volume, their density scaling as $\rho(R) \sim R^2$. In this case the time profile is given by

$$F(t) = F_0 \exp[-t/\tau_0 - 1.772n_q(t/\tau_0)^{1/2}(R_0/R_G)^3] \quad (9)$$

We note that in both models, since there are many quencher molecules within the relevant micellar volume, we can no longer extract the radius and quencher concentration separately, but only the total number of quenchers in the volume, $n_q(R_0/R_G)^2$ for the vesicle model or $n_q(R_0/R_G)^3$ for the polymer model.

Figure 12a shows our attempt to fit the aqueous solution of branched-tail ethoxylated sulfonate at $[surfactant] = 15$ mM, $[MG] = 0.1$ mM, at $[NaCl] = 0.5$ wt % with the vesicle model; the fluorescence time profile falls off more slowly than the predicted $\exp[-(t/\tau)^{1/2}]$. Figure 12b shows a successful fit to the same data with the polymeric model; the predicted $\exp[-(t/\tau)^{1/3}]$ provides a good representation of the data. Having fit at this acceptor dye concentration, doubling the acceptor dye concentration permits a comparison without adjustable parameters of the predicted to the measured decay profiles (Figure 12c). The fit is excellent.

Corroboration of these large structures is provided by NMR measurements. We look at the Na quadrupolar resonance.²⁵ Below the "transition", at $[NaCl] = 0.05$ g/dL, we obtain a narrow quadrupolar line as expected (Figure 13a). Above the transition, at $[NaCl] = 1.0$ g/dL, we see a broad line (Figure 13b) indicative of the slow diffusion of the large giant micelle, superposed on the narrower line.²⁶

Finally, we speculate as to a possible origin of the growth of these micelles. In addition to the usual location of the Na^+ ions in the electrical double layer associated with the sulfonate head groups of the surfactants, there are also "crown ether" sites formed by adjacent ethoxy groups on neighboring surfactants (Figure 14). Populating these "crown ether" sites with Na^+ ions (in the crown ethers these are known to be strongly binding sites) suppresses

(24) Dahanayake, M.; Cohem, A. W.; Rosen, M. J. *J. Phys. Chem.* **1986**, *90*, 2413.

(25) Wennerström, H.; Lindblom, G.; Lindman, B. *Chem. Scr.* **1974**, *6*, 97. Halle, B.; Wennerström, H. *J. Chem. Phys.* **1981**, *75*, 1928.

(26) Halle, B.; Carlström, G. *J. Phys. Chem.* **1981**, *85*, 2413.

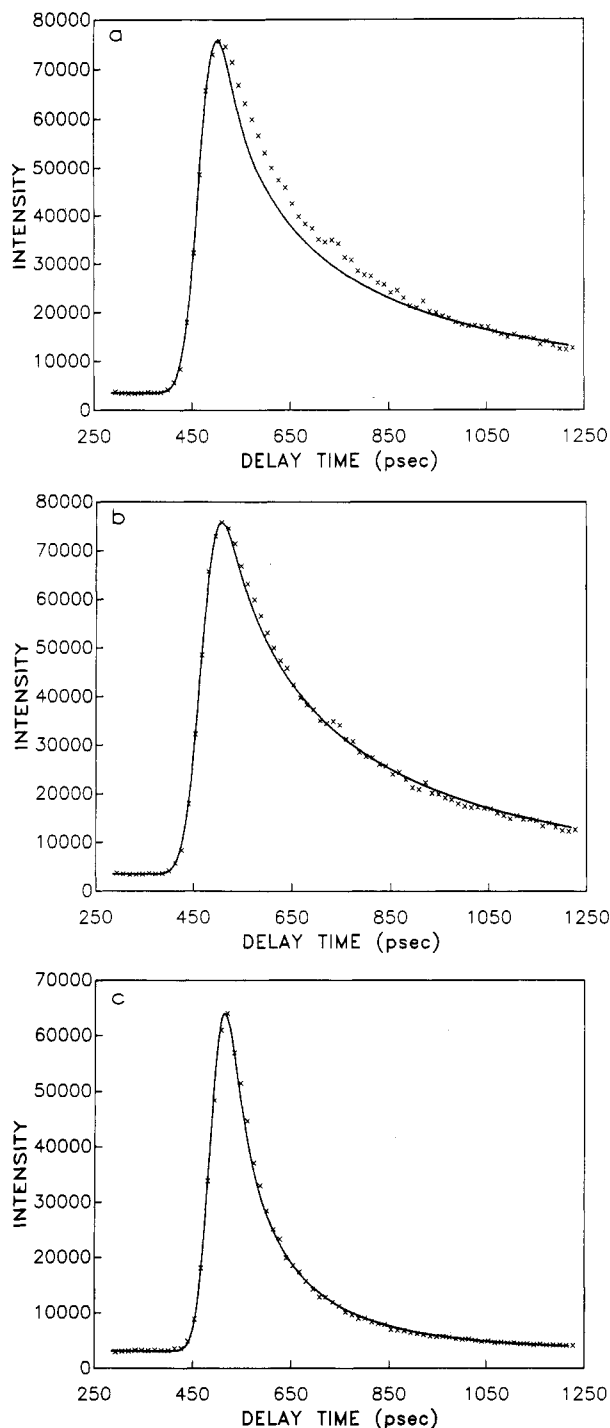


Figure 12. Fluorescence decay profile for rhodamine 6G solubilized in $C_{16}EO_2$ branched-tail ethoxylated sulfonate micelles ([surfactant] = 15 mM) at [NaCl] = 0.5%. (a) Unsatisfactory attempt to fit the vesicle micelle model time decay $\exp[-(t/\tau)^{1/2}]$ for [MG] = 0.1 mM. (b) Acceptable fit to the polymeric micelle model time decay $\exp[-(t/\tau)^{1/3}]$ for [MG] = 0.1 mM. (c) Agreement of theoretical prediction from fit (b) to the time decay for [MG] = 0.2 mM.

the randomness associated with the tight spherical micelle structure, and the spherical micelle is forced apart into a cylindrical structure. This cylindrical micelle can then grow indefinitely, and the cylinder then evolves into a flexible polymer. We note that this salinity-induced spherical micelle \rightarrow polymer micelle transition is qualitatively different from the usual salinity-induced sphere \rightarrow rod transition seen in many micelles. In those micelles, there is a shape evolution/deformation with salt, and only after the rod structure has formed does it grow. In the branched ethoxylated sulfonates we have investigated, the transition is very sharp with salt concentration, so that we have not

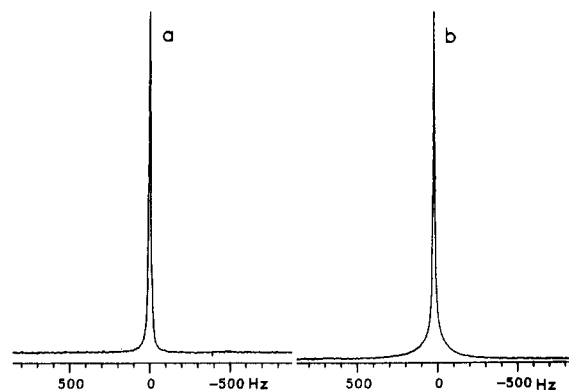


Figure 13. Na nuclear quadrupolar resonance of aqueous solution $C_{16}EO_2$ micelles: (a) At [NaCl] = 0.05 g/dL, the NMR line is narrow with width $\Gamma = 15$ Hz. (b) At [NaCl] = 0.5 g/dL, the NMR line is broad with actually two components of widths $\Gamma_1 = 27$ Hz and $\Gamma_2 = 200$ Hz with relative intensities $I_1/I_2 = 1.6$, indicative of the motional broadening due to the diffusion of the large aggregate.

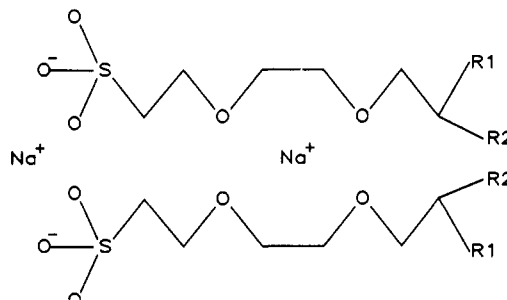


Figure 14. Proposed "crown ether" structure within ethoxylated sulfonate micelles to strongly bind Na^+ ions to induce the sphere to flexible polymer transition.

seen the short rigid rods but only the large flexible polymeric cylinders. It would thus appear that, while the usual double-layer binding of the counterions is responsible for the usual sphere \rightarrow rod micellar transitions, with the ethoxylated sulfonates we must invoke another counterion mechanism. We have proposed the tightly bound "crown ether" sites as possible candidate sites whose population would induce such a sudden transition.

6. Conclusion

Resonance energy transfer can be used to measure the distribution of probe dyes in a surfactant solution. The distribution of probe dyes can be controlled by selecting dyes with different chemical properties. We have applied resonance energy transfer to the measurement of the micellar size and aggregation number of a well-known surfactant system, SDS, and have compared our results with the literature value. We emphasize that the time scale involved in this measurement is shorter than the time required for significant molecular diffusion; therefore, the measurement is not affected by the microviscosity change of the micellar interface. We have extended these measurements to aqueous solutions of a branched-tail ethoxylated sulfonate, $C_{16}EO_2$, and have found evidence for a salinity-induced sphere \rightarrow polymeric micelle transition.

Note Added in Proof. Throughout this paper we have used a Förster radius, $R_0 \sim 52$ Å, for the rhodamine 6G/malachite green donor-acceptor pair, as measured^{6b} in homogeneous alcohol solution. We have recently performed²⁷ donor-acceptor resonance energy transfer experiments for this pair adsorbed onto polystyrene spheres, where we have measured $R_0 \sim 60$ Å. Sulfate ions, added to stabilize the surface charge on the latex spheres, probably act as binding sites for the cationic dyes, thereby shifting the fluorescence profile, $F(\nu)$, of the donor and the absorption profile, $A(\nu)$, of the acceptor, which is then reflected in an increase (1) in Förster radius. We expect similar shifts in the fluorescence

(27) Choi, K.-J.; Turkevich, L. A., unpublished results.

and absorption profiles of these cationic dyes bound to the sulfonate groups of the surfactants studied in this paper (SDS, C₁₆EO₂). As all lengths measured by resonance energy transfer scale with the Förster radius, we suspect that all the lengths reported in this paper should be augmented by 15%.

Acknowledgment. We thank T. Gustafson for assistance in setting up the synchronously pumped dye laser system used in this

study. We thank T. Hammond for the NMR study and R. Dorshow for the bulk light scattering study of the ethoxylated sulfonate. We thank D. Chernoff, E. Fendler, H. Scher, and R. Swofford for helpful discussions.

Registry No. SDS, 151-21-3; C₁₆EO₂, 113218-99-8; rhodamine 6G, 989-38-8; malachite green, 569-64-2; 2-[2-(2-hexyldecyloxy)ethoxy]ethanol, 113181-09-2; 1-iodo-2-[2-(2-hexyldecyloxy)ethoxy]ethanol, 113181-10-5.

The Sorption and Diffusion of Alkenes with Nonporous and Microporous Heteropoly Oxometalates

V. S. Nayak and J. B. Moffat*

Department of Chemistry and Guelph-Waterloo Centre for Graduate Work in Chemistry, University of Waterloo, Waterloo, Ontario, Canada N2L 3G1 (Received: April 28, 1987; In Final Form: July 14, 1987)

Sorption equilibrium and sorption kinetics of 1-hexene, 2,3-dimethyl-1-butene, 1-heptene, 1-octene, cyclohexene, and 4-methyl-1-cyclohexene have been studied at 293, 308, and 323 K on heteropoly compounds. The adsorption of alkenes is virtually irreversible on 12-tungstophosphoric acid (HPW), 12-tungstosilicic acid (HSiW), and 12-molybdophosphoric acid (HPMo), whereas that on the ammonium salts of these acids is reversible. The sorption capacities of the ammonium salts appear to be dependent upon the pore-size distribution and boiling points of the sorbates. The heats of sorption on the ammonium salts increase with increase in the boiling point of the sorbate. The diffusivities of alkenes decrease with increase in boiling point and kinetic diameter. The diffusivity of a particular alkene in different ammonium salts is in the order NHSiW > NHPMo > NHPW.

Introduction

Solids with porous structures and particularly those containing micropores are of special interest as heterogeneous catalysts in a variety of processes.^{1,2} While attention has been primarily focused on zeolites of various types, other microporous solids have been developed in the past several years. Recent work in this laboratory has shown that certain heteropoly oxometalates may be prepared with microporous structures.³⁻⁵ Unfortunately, however, little or no information is available on their sorption and diffusion properties. Since such data is important for the understanding of catalytic processes occurring on these microporous solids, a program to generate this information has been initiated in this laboratory.

Heteropoly oxometalates are ionic solids with high molecular weight cage-like anions. Of particular interest in the present work are those with Keggin structure. In these the anions consist of a central atom such as phosphorus to which are bonded four oxygen atoms arranged tetrahedrally. Twelve tetrahedra with oxygen atoms at their vertices and a peripheral metal atom such as tungsten envelop the central tetrahedron and share oxygen atoms with the latter and each other. Three types of oxygen atoms are found in the anion. One of these bridges the central and peripheral metal atoms and another two of the latter, while the terminal oxygen atom is bonded only to the peripheral metal atom and protrudes from the anion.

Earlier work from this laboratory has shown that 12-tungstophosphoric acid (H₃PW₁₂O₄₀) is an effective heterogeneous catalyst in the conversion of alcohols to hydrocarbons.⁶⁻⁸ However, the ammonium salt of this heteropoly oxometalate displays not only an enhanced activity in such processes as compared to the parent acid but produces primarily saturated hydrocarbons, in contrast to the olefinic products produced by the parent acid.^{8,9} Although the surface areas of the heteropoly acids are relatively low, molecules such as alcohols are evidently capable of penetrating into the bulk structure. Subsequent photoacoustic FTIR studies

in this laboratory have indeed shown that molecules such as ammonia, pyridine, and various alcohols are capable of interacting with both the peripheral and interior protons.¹⁰⁻¹⁷ Further work has shown that not only the ammonium salt of 12-tungsto-

(1) (a) Palekar, M. G.; Rajadhyaksha, R. A. *Catal. Rev.—Sci. Eng.* **1986**, *28*, 371. (b) Dewing, J.; Spencer, M. S.; Whittam, T. V. *Catal. Rev.—Sci. Eng.* **1985**, *27*, 461. (c) Kaeding, W. W.; Barle, G. C.; Wu, M. M. *Catal. Rev.—Sci. Eng.* **1984**, *26*, 597. (d) Chang, C. D. *Catal. Rev.—Sci. Eng.* **1983**, *25*, 1.

(2) (a) Flanigen, E. M. *Catal. Rev.—Sci. Eng.* **1984**, *26*, 483. (b) Rabo, J. A. *Catal. Rev.—Sci. Eng.* **1981**, *23*, 293. (c) Kerr, G. T. *Catal. Rev.—Sci. Eng.* **1981**, *23*, 281. (d) Haynes, H. W., Jr. *Catal. Rev.—Sci. Eng.* **1978**, *17*, 273.

(3) McMonagle, J. B.; Moffat, J. B. *J. Colloid Interface Sci.* **1984**, *101*, 479.

(4) Taylor, D. B.; McMonagle, J. B.; Moffat, J. B. *J. Colloid Interface Sci.* **1985**, *108*, 278.

(5) Moffat, J. B. *Polyhedron* **1986**, *5*, 261.

(6) Hayashi, H.; Moffat, J. B. *J. Catal.* **1982**, *77*, 473.

(7) Hayashi, H.; Moffat, J. B. *J. Catal.* **1983**, *81*, 61.

(8) Hayashi, H.; Moffat, J. B. In *Catalytic Conversion of Synthesis Gas and Alcohols to Chemicals*; Herman, R. G., Ed.; Plenum: New York, 1984; p 395.

(9) Hayashi, H.; Moffat, J. B. *J. Catal.* **1983**, *83*, 192.

(10) Highfield, J. G.; Hodnett, B. K.; McMonagle, J. B.; Moffat, J. B. In *Proceedings, 8th International Congress on Catalysis*; Verlag-Chemie: Weinheim, 1984; Vol. 5, p 611.

(11) Highfield, J. G.; Moffat, J. B. *J. Catal.* **1984**, *88*, 177.

(12) Moffat, J. B.; Highfield, J. G. In *Proceedings, 9th Canadian Symposium on Catalysis, Quebec City, 1984: Catalysis on the Energy Scene*; Kaliaguine, S.; Mabey, A., Ed.; Elsevier: Amsterdam, 1984.

(13) Highfield, J. G.; Moffat, J. B. *J. Catal.* **1984**, *89*, 185.

(14) Highfield, J. G.; Moffat, J. B. *J. Catal.* **1985**, *95*, 108.

(15) Moffat, J. B. In *Catalysis by Acids and Bases*; Imelik, B.; Naccache, C.; Courduria, G.; Ben Taario, Y.; Vadrine, J. C., Eds.; Elsevier: Amsterdam, 1985; p 17.

(16) Moffat, J. B. In *Preparation of Catalysts IV*; Studies in Surface Science and Catalysis 31; Delmon, B.; Grange, P.; Jacobs, P. A.; Poncelet, G., Eds.; Elsevier: Amsterdam, 1987; p 241.

(17) Moffat, J. B. In *Production of Fuel and Chemicals from Natural Gas*, University of Auckland, 1987; Bibby, D.; Chang, C. D., Eds.; Elsevier: Amsterdam, 1987.

* Author to whom correspondence should be addressed.